

Article

Lithospheric Architecture and Metallogenesis in Liaodong Peninsula, North China Craton: Insights from Zircon Hf-Nd Isotope Mapping

Zhichao Zhang ¹, Yuwang Wang ^{1,*}, Dedong Li ¹ and Chunkit Lai ² 

¹ Beijing Institute of Geology for Mineral Resources, Beijing 100012, China; ZZC_CUGB@126.com (Z.Z.); lidedong2005@126.com (D.L.)

² Faculty of Science, Universiti Brunei Darussalam, Gadong BE1410, Brunei; chunkit.lai@ubd.edu.bn

* Correspondence: wyw@cnnm.com

Received: 17 January 2019; Accepted: 8 March 2019; Published: 14 March 2019



Abstract: The Liaodong Peninsula is an important mineral province in northern China. Elucidating its lithospheric architecture and structural evolution is important for gold metallogenic research and exploration in the region. In this study, Hf-Nd isotope maps from magmatic rocks are constructed and compared to geological maps to correlate isotopic signatures with geological features. It is found that gold deposits of different age periods in Liaodong are located in areas with specific $\epsilon\text{Hf}(t)$ and ϵNd ranges (Triassic: from -8 to -4 and from -12 to -8 , Jurassic: from -22 to -8 and from -14 to -8 , Cretaceous: from -12 to -10 and from -22 to -20), respectively. This may reflect that when the Paleo-Pacific plate was subducted beneath the North China Craton, the magma was derived from the juvenile lower crust and the ancient lower crust, and formed the low-to-moderate hydrothermal Au-(Ag) and Pb-Zn deposits in the Triassic. In the Jurassic, continued subduction may have led to lithospheric thickening. Subsequently, the magma from the ancient lower crust upwelled and formed low-to-moderate hydrothermal Au deposits and porphyry Mo deposits. In the Cretaceous, crustal delamination may have taken place. The magma from the ancient lower crust upwelled and formed various low-to-moderate hydrothermal Au deposits.

Keywords: lithospheric architecture; metallogenesis; Hf-Nd isotopic mapping; Liaodong Peninsula; North China Craton

1. Introduction

The North China Craton (NCC), containing the Liaodong and Jiaodong gold provinces, is the top gold producer in northeast Asia [1–6]. The Liaodong Peninsula is located between the Yalujiang and TanLu fault zones (Figure 1) [7–9] and represents an important mineral province in the NCC. The peninsula has undergone complex magmato-tectonic modifications, during which many important polymetallic (Pb-Zn, Au, Ag, and Mo) deposits have been formed (Figures 1 and 2) [10,11]. Most of these deposits are interpreted to be genetically linked with granitoid in the peninsula [11]. Granitoid in the Liaodong peninsula include the diorite and the granite that formed in the Paleoproterozoic, Permian, Jurassic, and Cretaceous [7,12,13]. These many phases of magmatism provide a window into the study of the lithospheric architecture and its control on metallogenesis.

Tectonic evolution and the characteristics of gold deposits in Liaodong and Jiaodong are similar [14–18]; however, whether or not the lithospheric architecture played a role in controlling the tectonic evolution and gold ore formation remains poorly understood.

The Hf and Nd isotopes are powerful tools to trace the nature of basement rocks and the age of the continental crust [19–21], and Hf-Nd isotope mapping has been used to reveal the lithospheric architecture and evolution, and their control on the distribution of mineral deposits [22–29].

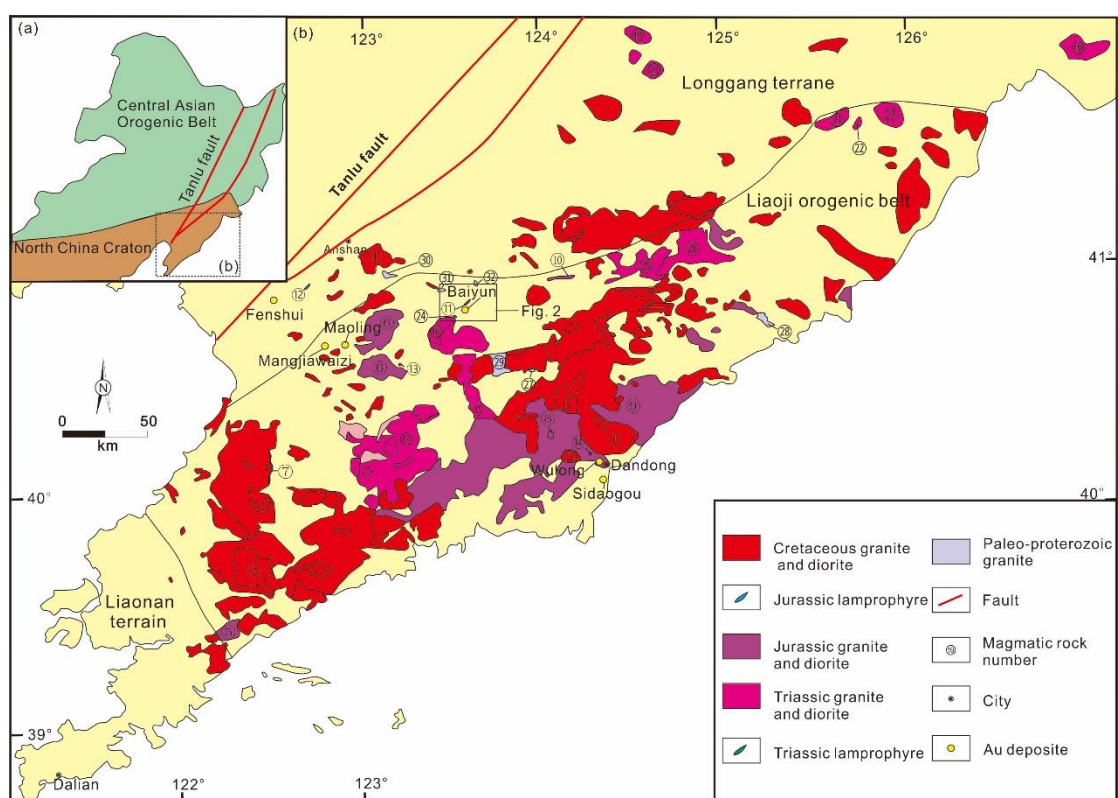


Figure 1. (a) Simplified tectonic map of the Liaodong Peninsula showing the major suture zones and blocks. (b) Geological map of the Liaodong Peninsula showing the distribution of magmatic rocks, and the locations of major mineral deposits [30].

In this study, we summarize the spatial distribution, age, and geochemical and isotopic data of the Paleoproterozoic to Cretaceous magmatic rocks in the Liaodong Peninsula, and we use Hf-Nd isotope mapping to reveal the crustal architecture and its controls on the regional mineralization.

2. Geological Setting

2.1. Regional Tectonics

The Liaodong Peninsula is located in the eastern margin of the NCC (Figure 1). It is bounded by the Yalujiang fault in the east and by the Tanlu fault in the north [31,32]. The Liaodong Peninsula can also be subdivided into the Longgang terrane in the north, the Liaoji orogenic belt in the middle, and the Langlin terrane in the south. This study only focuses on the Longgang terrane and the Liaoji orogenic belt. The Longgang terrane is composed of Archean to Paleoproterozoic basement rocks, and unmetamorphosed Mesoproterozoic to Cenozoic sedimentary and volcanic rocks [7]. The Liaoji orogenic belt consists mainly of Paleoproterozoic to Cretaceous magmatic rocks. In the Longgang terrane, the Paleoproterozoic sequences are missing, and the magmatic rocks are largely Triassic (Figure 3) [33].

2.2. Magmatism

The Liaodong Peninsula consists of Paleoproterozoic granite, Triassic granite and diorite, Jurassic granite and diorite, and Cretaceous granite and diorite (Table 1 and Table S1) (Figures 4 and 5) [34–39]. During the Paleoproterozoic, the voluminous granitoid and the mafic intrusions in the peninsula were emplaced (Figure 5) and then metamorphosed at 1.93 Ga [40], marking the cratonization of the NCC eastern block. The Triassic magmatism is characterized by metaluminous mafic and felsic magmatic rocks (Figure 5), which are also identified in the southern Liaodong Peninsula [7,30]. Late Mesozoic

intrusive rocks include Jurassic (180–153 Ma) ductile-deformed, peraluminous/metaluminous granite (Figure 5), and undeformed to slightly deformed early Cretaceous (131–120 Ma) metaluminous granite and diorite (Figure 5) [7,41,42].

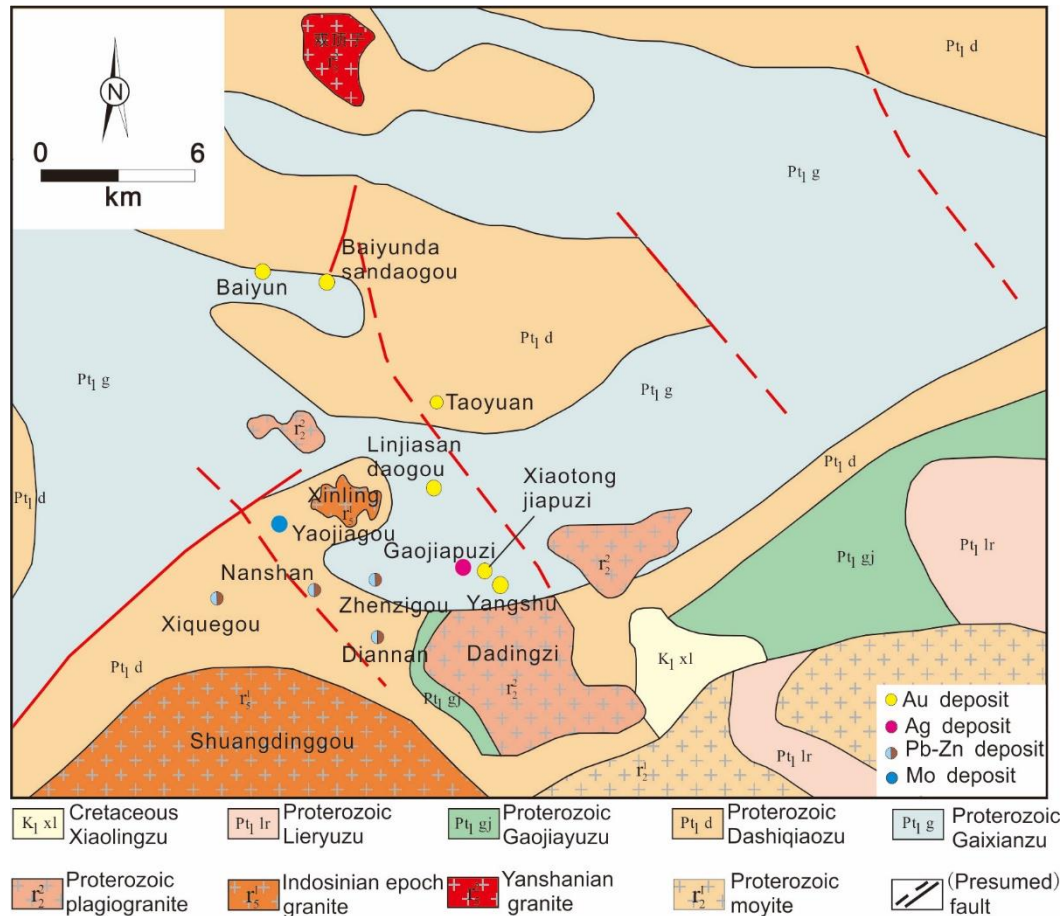


Figure 2. Simplified geologic map of the Qingchengzi orefield showing the distribution of deposits [11].

2.3. Mineralization

The Liaodong Peninsula contains Pb-Zn, Au, Ag, and Mo polymetallic deposits, which are mainly distributed in the Qingchengzi, Wulong, and Maoling orefields (Figure 1) (Table 2) [11,43,44]. The Qingchengzi orefield is in the northern part of the Liaodong Peninsula, which hosts a number of magmatic-hydrothermal (low-to-moderate hydrothermal) Au-(Ag) and Pb-Zn deposits and porphyry Mo deposits (Figure 2) [45,46]. The magmatic-hydrothermal Au-(Ag) deposits were mainly formed in the Triassic (225–240 Ma), as exemplified by the Baiyun and Yangshu deposits (Table 2). The mineralization of these deposits has been correlated to the granite and the diorite, which are the result of lithospheric thinning associated with the Paleo-Pacific plate subduction [30,35]. The magmatic-hydrothermal Pb-Zn deposits (e.g., Xiquegou and Zhenzigou) were also formed in the Triassic (221–232 Ma), whilst the Yaojiagou porphyry Mo deposit was formed in the Jurassic (168 Ma). The mineralization of these Pb-Zn deposits has been correlated to the granite and the diorite, and that of the Mo deposit has been correlated to the granite. The Pb-Zn and Mo deposits have been correlated to large-scale delamination [7,35].

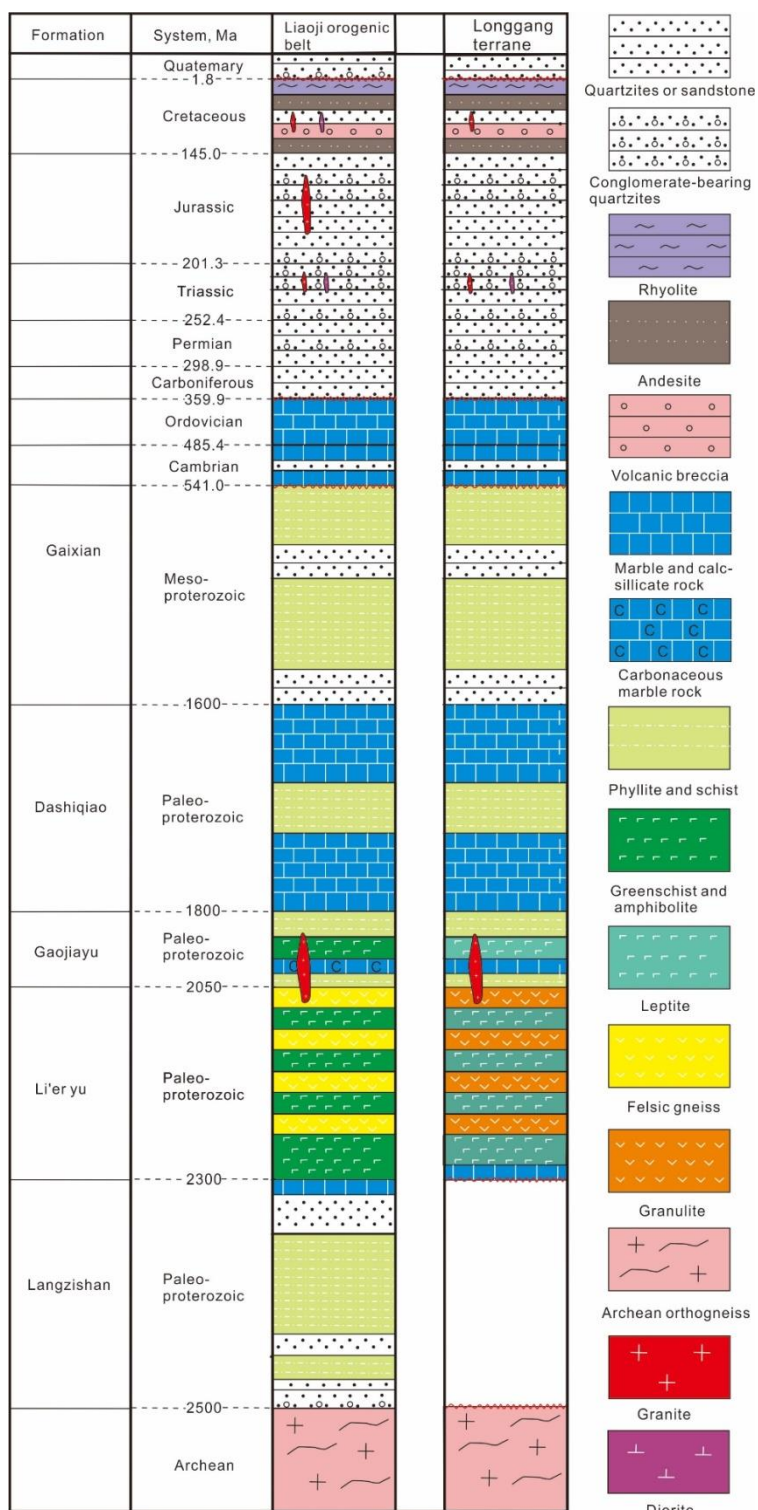


Figure 3. Stratigraphic columns showing the basement rocks, sedimentary cover, and magmatic history of the Longgang Terrane and the Liaoji orogenic belt.

Table 1. Zircon U-Pb ages for the magmatic rocks from the Liaodong Peninsula.

Period	No.	Pluton	Phase	Age/Ma	Sample	Method	References
Cretaceous	1	Wulongbei	Quartz diorite	126–127	Zircon	SHRIMP U-Pb	[7]
	2	Sanguliu	Porphyritic granite	125 ± 3	Zircon	SHRIMP U-Pb	[7]
	3	Yinmawanshan	Gneissic granodiorite	122 ± 2	Zircon	LA-ICP-MS U-Pb	[7]
		Yinmawanshan	Monzogranite (dike)	124 ± 5	Zircon	LA-ICP-MS U-Pb	[7]
		Yinmawanshan	Monzogranite	122 ± 6	Zircon	LA-ICP-MS U-Pb	[7]
	4	Qianshan	Granite	126 ± 2	Zircon	LA-ICP-MS U-Pb	[32]
Jurassic	5	Xiaoheshan	Granodiorite	173–174 ± 4	Zircon	LA-ICP-MS U-Pb	[7]
	6	Hanjjialing	Granodiorite	179 ± 3	Zircon	LA-ICP-MS U-Pb	[7]
			Monzogranite	164 ± 4	Zircon	LA-ICP-MS U-Pb	[7]
	7	Yutun	Mylonitic granite	157 ± 3	Zircon	LA-ICP-MS U-Pb	[7]
	8	Heigou	Monzogranite	161 ± 6, 163 ± 7	Zircon	LA-ICP-MS U-Pb	[7]
	9	Jiuliancheng	Monzogranite	156 ± 3	Zircon	LA-ICP-MS U-Pb	[7]
	10	Gaoliduntai	Plagiogranite	156 ± 5	Zircon	LA-ICP-MS U-Pb	[7]
	11	Baiyun gold mine	Porphyritic dyke	168 ± 3	Zircon	LA-ICP-MS U-Pb	[7]
	12	Huaziyu	Lamprophyres	155 ± 4	Zircon	LA-ICP-MS U-Pb	[47]
	13	Waling	Monzonitic granite	162.4 ± 1.9	Zircon	SHRIMP U-Pb	[36]
	14	Dandong	Granite	157–167	Zircon	LA-ICP-MS U-Pb	[14]
Triassic	15	Shuangdinggou	biotite monzogranite	224.2 ± 1.2	Zircon	LA-ICP-MS U-Pb	[9]
	16	Xinling	Granites	225.3 ± 1.8	Zircon	SHRIMP U-Pb	[8]
	17	Xiuyan	Monzogranite	210 ± 1	Zircon	LA-ICP-MS U-Pb	[30]
			Monzogranite	224 ± 2	Zircon	SIMS	[12]
	18	Nankouqian	Monzogranite	221 ± 2	Zircon	LA-ICP-MS U-Pb	[12]
Granite			224 ± 1	Zircon	LA-ICP-MS U-Pb	[48]	

Table 1. Cont.

Period	No.	Pluton	Phase	Age/Ma	Sample	Method	References
Triassic	19	Mayihe	Pyroxene diorite	222 ± 2	Zircon	SIMS	[12]
			Pyroxene syenodiorite	223 ± 2	Zircon	SIMS	[12]
			Fine-grained diorite	222 ± 2	Zircon	SIMS	[12]
			Biotite monzogranite	220 ± 2, 223 ± 3, 221 ± 2	Zircon	LA-ICP-MS U-Pb	[12]
	20	Xidadingzi	Monzogranite	220 ± 2, 221 ± 2	Zircon	LA-ICP-MS U-Pb	[12]
	21	Chaxinzi	Monzogranite	222 ± 2, 219 ± 2	Zircon	LA-ICP-MS U-Pb	[12]
			Diorite	219 ± 4	Zircon	LA-ICP-MS U-Pb	[12]
			Monzodiorite	222 ± 2	Zircon	LA-ICP-MS U-Pb	[12]
			Diorite	221 ± 2	Zircon	SIMS	[12]
			Granodiorite	222 ± 1	Zircon	SIMS	[12]
	22	Xiaoweishahe	Granodiorite	218 ± 2	Zircon	LA-ICP-MS U-Pb	[12]
			Quartz diorite	220 ± 2, 219 ± 4	Zircon	LA-ICP-MS U-Pb	[12]
	23	Longtou	Granodiorite	224 ± 2	Zircon	SIMS	[12]
			Granodiorite	220 ± 2	Zircon	LA-ICP-MS U-Pb	[12]
			Fine-grained granite	221 ± 2	Zircon	LA-ICP-MS U-Pb	[12]
	24	Qingchengzi	Lamprophyres	224–230	Zircon	LA-ICP-MS U-Pb	[9]
25	Saima	Syenite	222 ± 3.4	Zircon	LA-ICP-MS U-Pb	[49]	
		Syenite	221 ± 2.3	Zircon	LA-ICP-MS U-Pb	[49]	
26	Bailinchuan	Syenite	221 ± 2.3	Zircon	LA-ICP-MS U-Pb	[49]	
Paleo-proterozoic	27	Jiguanshan	Granite	2175 ± 13	Zircon	SHRIMP U-Pb	[38,50]
	28	Laoheishan	Granite	2166 ± 14	Zircon	SHRIMP U-Pb	[38,50]
	29	Dadingzi	Granite	1869 ± 16	Zircon	SHRIMP U-Pb	[39]
	30	Wuleishan	Granite	1830.5 ± 5.9	Zircon	SHRIMP U-Pb	[39]
	31	Simenzi	Granite	2157 ± 14	Zircon	SHRIMP U-Pb	[39]
	32	Gujiapu	Granite	2169 ± 11	Zircon	SHRIMP U-Pb	[39]

Table 2. Summary of the geological characteristics of major ore deposits in the Liaodong Peninsula.

Number	Deposits	Orefield	Type	Metallic Comm.	Tonnage (t)	Grade	Host Rock	Age (Ma)	Data Source
1	Zhenzigou	Qingchengzi	Magmatic hydrothermal	Pb-Zn		0.37, 450	Marble, Amphibolite, Schist	221	[8,51]
2	Nanshan	Qingchengzi	Magmatic hydrothermal	Pb-Zn		0.5, 153		227	[9,11]
3	Diannan	Qingchengzi	Magmatic hydrothermal	Pb-Zn		0.08, 650		232	[11]
4	Xiquegou	Qingchengzi	Magmatic hydrothermal	Pb-Zn		0.28, 250		225	[8,11]
5	Baiyun	Qingchengzi	Magmatic hydrothermal	Au	31.7	2.85 g/t	Metamorphic rock and quartz veins	225	[10,11]
6	Xiaotongjiapuzi	Qingchengzi	Magmatic hydrothermal	Au-Ag	20–50	0.07~2.92, 0.14~6.12	Marble	239	[11,43,52,53]
7	Gaojiapuzi	Qingchengzi	Magmatic hydrothermal	Ag		312	Marble	240	[11,45,52,54]
8	Yangshu	Qingchengzi	Magmatic hydrothermal	Au-Ag	3.72	1.61, 3.72	Metamorphic rock and marble		[11,55]
9	Taoyuan	Qingchengzi	Magmatic hydrothermal	Au-Ag		0.005~0.06, 0.0025~0.1	Metamorphic rock		[11,56]
10	Baiyundasandaogou	Qingchengzi	Magmatic hydrothermal	Au-Ag		7.28, 1.28			[11,54]
11	Linjiasandaogou	Qingchengzi	Magmatic hydrothermal	Au		0.031, 0.034	Metamorphic rock		[11,56]
12	Yaojiagou	Qingchengzi	porphyry	Mo		0.34	Metamorphic rock and skarn	168	[57,58]
13	Sidaogou	Wulong	Magmatic hydrothermal	Au	20–50		Metamorphic rock		[43]
14	Wulong	Wulong	Magmatic hydrothermal	Au	>40		Metamorphic rock and quartz veins	122	[43,59]
15	Wangjiawaizi	Maoling	Magmatic hydrothermal	Au-Ag	>5	8.9, 16.9	Metamorphic rock, quartz veins and Breccia		[60]
16	Maoling	Maoling	Magmatic hydrothermal	Au	25	3.2 g/t	Metamorphic rock and quartz veins	196	[44]
17	Fenshui	Maoling	Magmatic hydrothermal	Au	1.8	3~5	Quartz veins	186	[61]

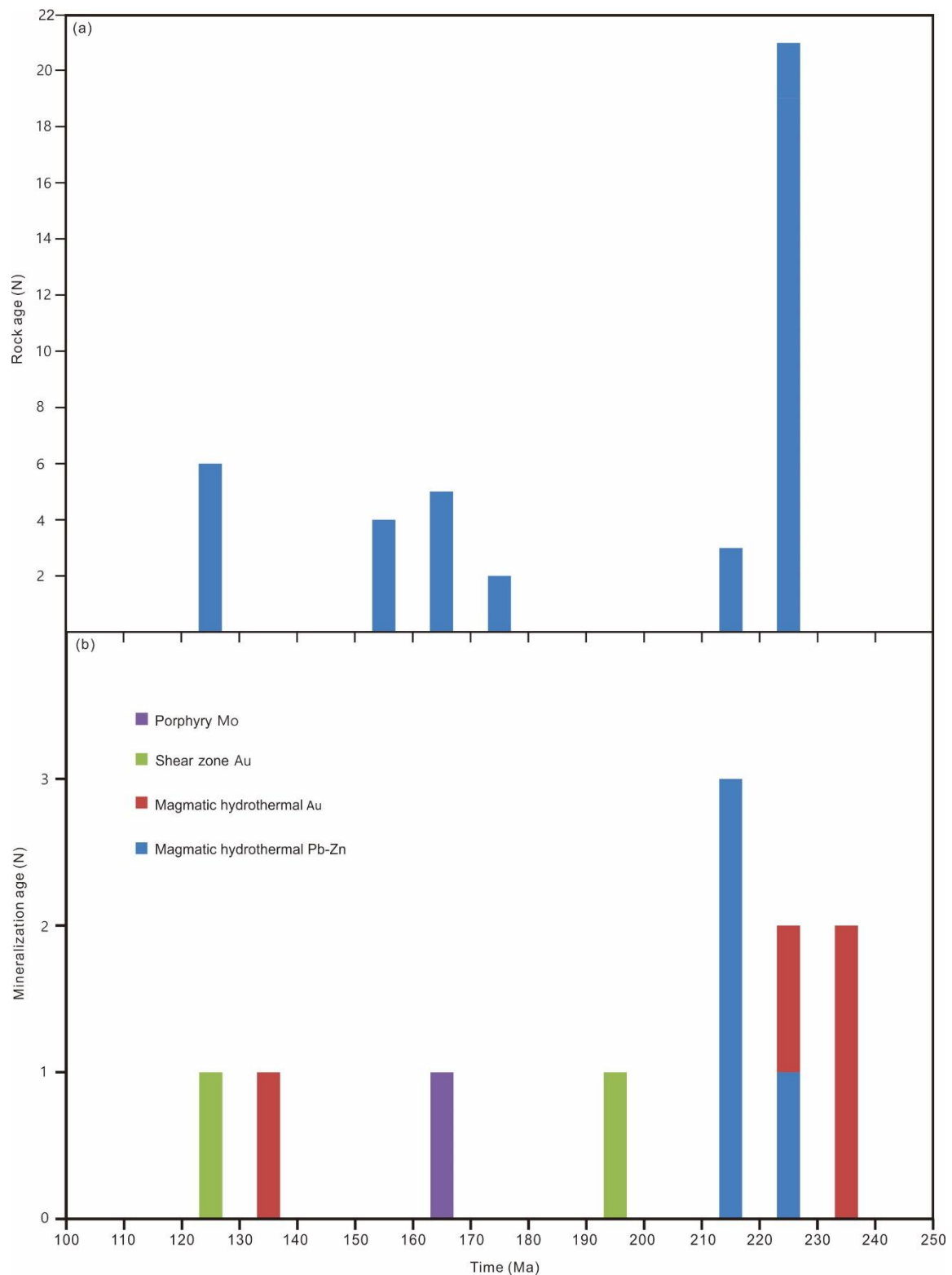


Figure 4. (a) Histogram of geochronological dating of zircon U-Pb ages of magmatic rocks. (b) Histogram of geochronological dating of mineralization.

The Wulong orefield contains the Wulong and Sidaogou magmatic-hydrothermal (low-to-moderate hydrothermal) Au deposits. The largest Wulong deposit was formed at 122 Ma [62], whilst the Sidaogou deposit in southern Liaodong has no reliable mineralization age data.

The Maoling orefield contains the Jurassic, Maoling, Fenshui, and Wangjiawaizi magmatic-hydrothermal (low-to-moderate hydrothermal) Au deposits (186–189 Ma) [44,60,61].

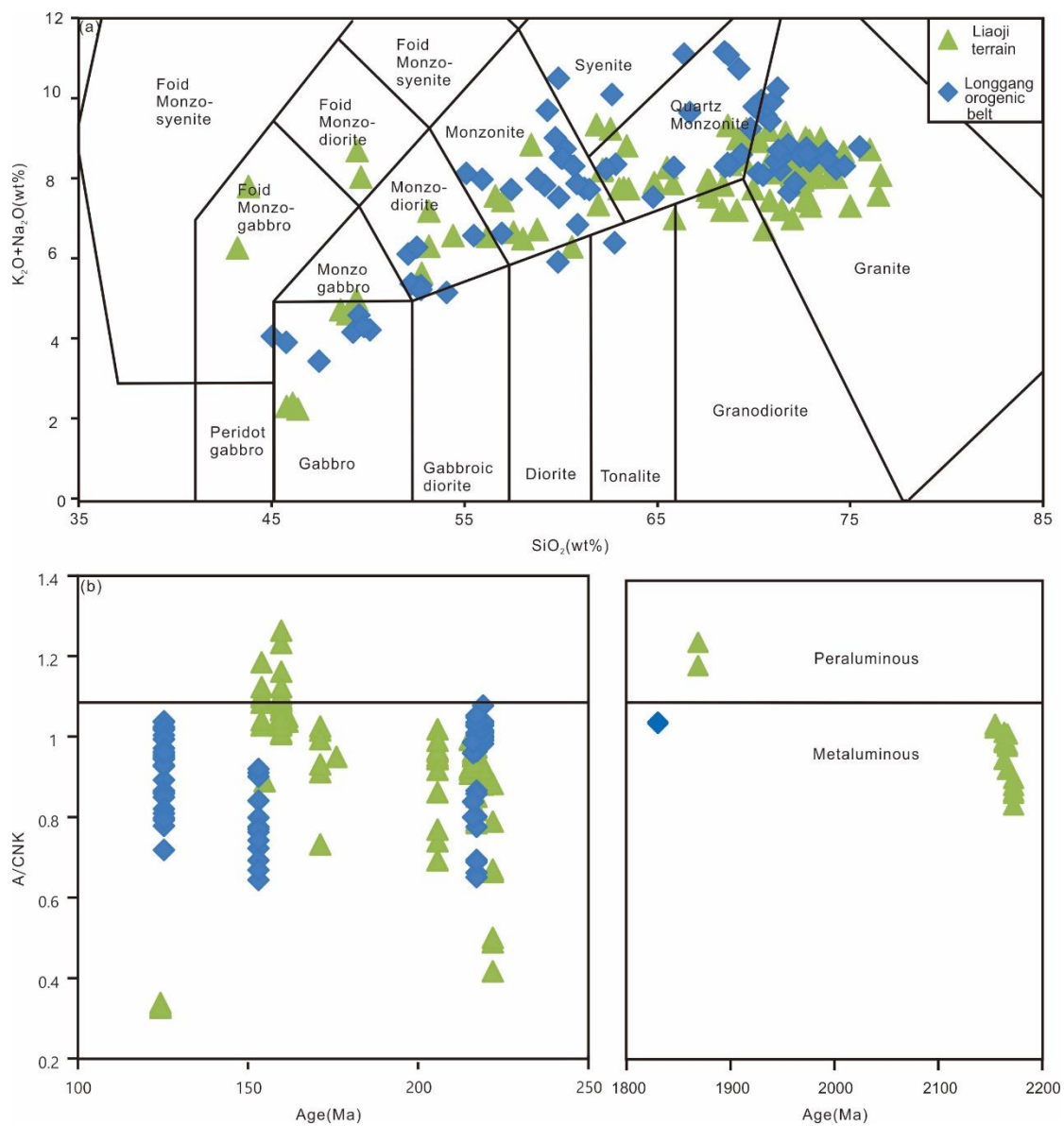


Figure 5. (a) Total alkali ($\text{Na}_2\text{O} + \text{K}_2\text{O}$) versus SiO_2 diagram. (b) A/CNK (molecular $\text{Al}_2\text{O}_3 / (\text{CaO} + \text{Na}_2\text{O} + \text{K}_2\text{O})$) versus zircon U-Pb age diagram. Dates are in Table 1 and the Supplementary Material Table S1.

3. Methods

Published zircon U-Pb age and Hf isotope data (35 samples) and whole-rock Sr-Nd isotope data (35 samples) from the Liaodong Peninsula have been compiled. Data compiled were from Paleoproterozoic to Cretaceous rocks, including (porphyritic) granite, monzogranite, lamprophyre, plagiogranite, (gneissic) granodiorite, (quartz) diorite, and syenodiorite. New data were also added in this study via collecting and analyzing (for zircon Lu-Hf isotopes) samples from the Qingchengzi orefield. The Zircon U-Pb age of the Miaonangou gabbro near the Baiyun gold deposit was in 1252 Ma [63], and the porphyrie (diorite, monzogranite) in the Baiyun deposit were emplaced in 229–222 Ma [63,64]. The Gujiapuzi granite porphyry in the Qingchengzi orefield was in 219 Ma [63].

Zircon Hf isotopes were analyzed using a 193-nm laser ablation (LA) system attached to a Neptune multi-collector (MC)-ICP-MS (Laboratory of Isotope Geology, Tianjin Institute of Geology and Mineral

Resources, China). A laser pulse (100 mJ energy, 10 Hz frequency, 50 μm beam size) was used for the laser ablation [65]. Isobaric interference of ^{176}Lu on ^{176}Hf was corrected on the basis of the measured ^{175}Lu value and the recommended $^{176}\text{Lu}/^{175}\text{Lu}$ ratio of 0.02655. Similarly, the $^{176}\text{Yb}/^{172}\text{Yb}$ value of 0.5887 and mean β Yb value obtained during Hf analysis on the same spot were used for interference correction of ^{176}Yb on ^{176}Hf [66,67]. A ^{176}Lu decay constant of $1.865 \times 10^{-11}\text{-year}^{-1}$ [68] and the chondritic ratios of $^{176}\text{Hf}/^{177}\text{Hf} = 0.282785$ and $^{176}\text{Lu}/^{177}\text{Hf} = 0.0336$ [69] were used to calculate the $\epsilon\text{Hf}(t)$ values [70–72].

The Hf-Nd contour maps were produced using the inverse distance weighted interpolation method in the MapGIS 6.7 (Manufacturer is Zondy Cyber, Wuhan, China) program to contour the Hf and Nd dataset, which accounts for the distance between sample points in the most representative manner [73–75]. In order to produce the most robust spatial representation of the isotopic dataset, this method used 12 nearest neighbors at a power of 2 following [24]. All isotope data were grouped by the geometric interval method designated for class breaks. This ensured that each class range had approximately the same number of values, and that the change between intervals was fairly consistent. All point data shown in the contour maps represent the median for a range of Hf-Nd isotope values from an individual sample, which helped to minimize data anomalies [23,28,76].

4. Results

4.1. Zircon Hf Isotope Features

Zircon $\epsilon\text{Hf}(t)$ values of the Longgang terrane vary from -18.9 to 5.8 (average -3.3), and the old crustal Hf model ages (T_{DM}^{C}) range from 994 to 2058 Ma (average 1349 Ma). Zircon $\epsilon\text{Hf}(t)$ values of the Liaoji orogenic belt vary from -33 to 11.7 (average -11.4), and the T_{DM}^{C} range from 763 to 2785 Ma (average 1449 Ma).

For the Paleoproterozoic rocks, the $\epsilon\text{Hf}(t)$ and T_{DM}^{C} ranged from -17.4 to 7.9 (average -0.8) and from 2036 to 3874 Ma (average 2948 Ma), respectively. For the Triassic rocks, the zircon $\epsilon\text{Hf}(t)$ and T_{DM}^{C} ranged from -18.9 to 5.2 (average -11.5) and from 763 to 2613 Ma (average 1422 Ma), respectively. For the Jurassic rocks, the zircon $\epsilon\text{Hf}(t)$ and T_{DM}^{C} range from -28.9 to -1.1 (average -16.3) and from 1505 to 2785 Ma (average 2041 Ma), respectively (Table S2).

Contour maps of the zircon $\epsilon\text{Hf}(t)$ values for the Paleoproterozoic-Cretaceous Liaodong magmatic rocks show four high $\epsilon\text{Hf}(t)$ domains and two low $\epsilon\text{Hf}(t)$ domains, among which two high $\epsilon\text{Hf}(t)$ domains are in the Longgang terrane, and the other two are in the Liaoji orogenic belt (Figure 6). There are two low $\epsilon\text{Hf}(t)$ domains in the Longgang terrane and the Liaoji orogenic belt, respectively (Figure 6).

4.2. Whole-Rock Sr-Nd Isotope Features

The $(^{87}\text{Sr}/^{86}\text{Sr})_i$ ratios of the Liaoji orogenic belt and the Longgang terrane range from 0.7044 to 0.7215 (average 0.7098) and from 0.7037 to 0.7306 (average 0.7085), respectively. The ϵNd values of the Liaoji belt and the Longgang terrane range from -24.9 to -0.9 (average -14.1) and from -18.9 to 3.82 (average -5.1), respectively (Table S3).

For the Cretaceous rocks, the ϵNd and T_{DM} values range from -19.3 to -11.9 (average -15.1) and from 1388 to 2191 Ma (average 1831 Ma). For the Jurassic rocks, the $(^{87}\text{Sr}/^{86}\text{Sr})_i$, ϵNd , and T_{DM} values range from 0.7044 to 0.7215 (average 0.7104), -24.9 to -9.6 (average -11.2), and 1110 to 2826 Ma (average 1888 Ma), respectively. For the Triassic rocks, the $(^{87}\text{Sr}/^{86}\text{Sr})_i$, ϵNd , and T_{DM} values range from 0.7037 to 0.7306 (average 0.7082), -18.9 to 3.82 (average -9.5), and 726 to 2290 Ma (average 1541 Ma), respectively. For the Paleoproterozoic rocks, the ϵNd and T_{DM} values range from -16.2 to -0.9 (average -5.8) and from 2480 to 2813 Ma (average 2279 Ma), respectively (Table S3).

The Contour maps of whole-rock Nd isotopes for the Paleoproterozoic-Cretaceous magmatic rocks show three high ϵNd domains and four low ϵNd domains in the region. One high ϵNd and one

low ϵ_{Nd} domain are in the Longgang terrane, and the other two high ϵ_{Nd} domains and three low ϵ_{Nd} domains are in the Liaoji belt (Figure 7).

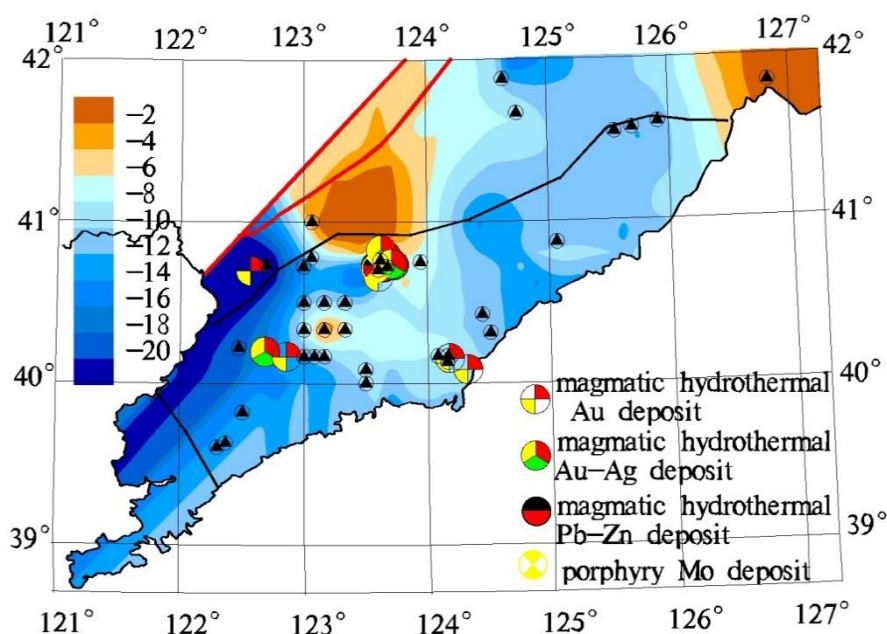


Figure 6. Contour maps of the Hf isotope for the magmatic rocks in the Liaodong Peninsula. Data are from Supplementary Material Table S2.

5. Discussion

5.1. Lithospheric Architecture of the Liaodong Peninsula

In the Longgang terrane, there are two domains characterized by high ϵ_{Hf} values (Figure 6), that are present in the area of the Triassic and Paleoproterozoic granite and diorite (Figure 1) and indicate that the granite and the diorite of this area are derived from the mantle or juvenile lower crust. There are also two domains characterized by low- ϵ_{Hf} in the Longgang terrane (Figure 6), that indicate the magmatic rocks of this area are derived from the lower crust. In the Liaoji orogenic belt, there are two domains characterized by high- ϵ_{Hf} (Figure 6), which are present in the area of Triassic and Paleoproterozoic granite and diorite (Figure 1), and indicate that the rocks are derived from the mantle or juvenile lower crust. There are also two low- ϵ_{Hf} domains in the Liaoji orogenic belt (Figure 6) that indicate the crustal origin of the magmatic rocks in this area.

There is one high ϵ_{Nd} domain in the Longgang terrane, and there are two high ϵ_{Nd} domains in the Liaoji orogenic belt (Figure 7). However, the ϵ_{Nd} values of the two domains in the Liaoji orogenic belt are still below zero. Therefore, the magmatic rocks in the Liaoji orogenic belt are derived from the lower crust. The high ϵ_{Nd} domain in the Longgang terrane is present in the area of the Triassic granite and the diorite (Figure 7). This also can indicate that the granite and the diorite are mostly derived from the mantle or juvenile lower crust.

In the Longgang terrane, the area of the Triassic granite and the diorite with high- ϵ_{Hf} and high- ϵ_{Nd} shows that the magmatic rocks are derived from the juvenile lower crust (Figure 8). The high $(^{87}\text{Sr}/^{86}\text{Sr})_i$ ratios also support this evidence (Figure 9). The area of Paleoproterozoic granite and diorite with high- ϵ_{Hf} in the Longgang terrane shows that the magmatic rocks are from juvenile lower crust (Figure 8). In the Liaoji orogenic belt, the area of Triassic granite and diorite with high- ϵ_{Hf} shows that the magmatic rocks are from the juvenile lower crust (Figure 8). The area of Paleoproterozoic granite and diorite with high- ϵ_{Hf} shows that the magmatic rocks are from the depleted mantle (Figure 8).

In the Paleoproterozoic, the Tanlu fault may have experienced dextral shear movement, and the intense regional extension creating the Liaodong rift valley [77], although the actual timing and number of stages (argued variably from four to six) of the rifting process remain controversial. The timing of rifting is also variably attributed from 2.3 to 1.7 Ga or from 2.3 to 1.8 Ga [9,77]. The magmatic rocks in the Longgang terrane are from the juvenile lower crust and the ancient lower crust, but the magmatic rocks in the Liaoji orogenic belt are from the depleted mantle and the ancient lower crust (Figures 6–8).

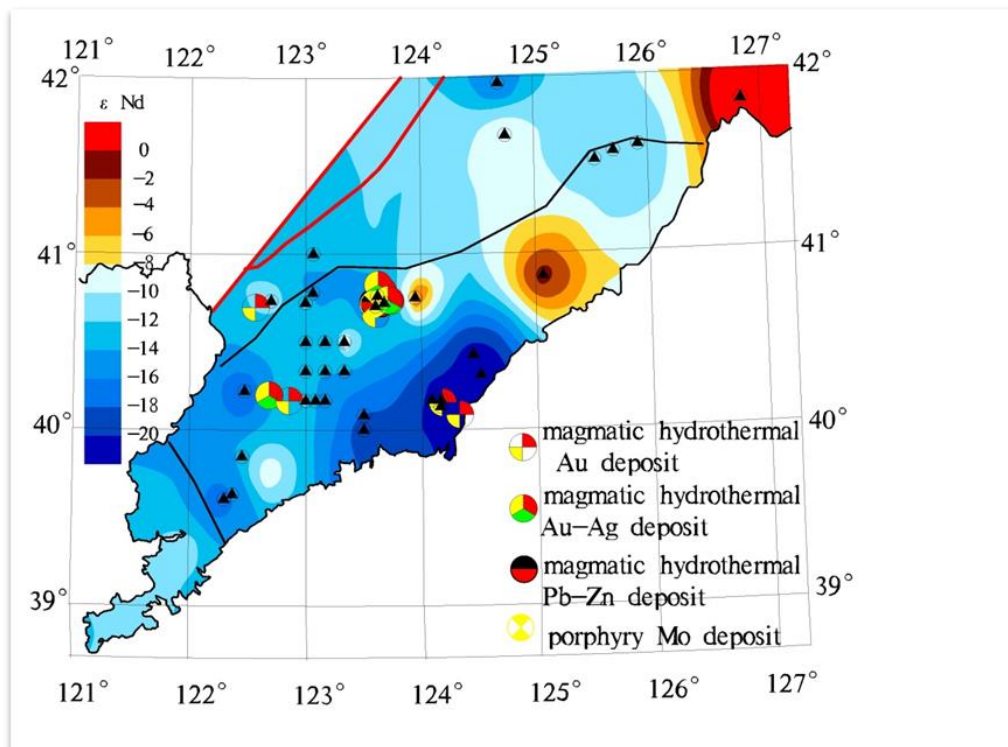


Figure 7. Contour maps of the Nd isotope for the magmatic rocks in the Liaodong Peninsula. Data are from Supplementary Material Table S3.

In the Mesozoic, the Liaodong Peninsula was likely in a post-collisional extensional setting [9,78,79], and the Paleo-Pacific plate may have subducted beneath the NCC [6,9]. Zircon and monazite SHRIMP U-Pb dating suggested that the continental collision took place in 220–240 Ma [80–82]. In the Triassic, the collision between North China and Paleo-Pacific plate likely caused the lithospheric thickening in the Liaoji rift [30,35,83]. The Triassic magmatic rocks are derived from the juvenile lower crust and the ancient lower crust (Figures 6–9). The rocks have positive whole rock $\epsilon\text{Nd}(t)$ and zircon $\epsilon\text{Hf}(t)$ values, indicating a juvenile lower crustal source. In addition, the Triassic magmatic rocks with high SiO_2 contents and low MgO concentrations have strong negative and variable whole rock $\epsilon\text{Nd}(t)$ and zircon $\epsilon\text{Hf}(t)$ values, indicating that they were derived from partial melting of the ancient lower crustal materials with involvement of mantle components [12]. In the Jurassic, the lithospheric thickening continued [1,84–88]. The sources of the magmatic rocks are from the ancient lower crust (Figures 6–9). The rocks with strong negative and variable whole rock $\epsilon\text{Nd}(t)$ and zircon $\epsilon\text{Hf}(t)$ values indicate that they were derived from partial melting of the Precambrian basement [7]. In the Cretaceous, large-scale delamination may have taken place [35,89]. The magmatic rocks have the same characteristics of whole rock $\epsilon\text{Nd}(t)$ and zircon $\epsilon\text{Hf}(t)$ values as those of Cretaceous magmatic rocks. Therefore, the sources of the magmatic rocks are also derived from the ancient lower crust (Figures 6, 7 and 9).

5.2. Regional Tectonic Evolution and Relation to Mineralization

The Triassic is the principal metallogenic epoch in Liaodong. Deposits formed in the Triassic include the Zhenzigou, Nanshan, Diannan, and Xiquegou low-to-moderate hydrothermal Pb-Zn deposits, the Baiyun and Xiaotongjiapuzi low-to-moderate hydrothermal Au-Ag deposits, and the Gaojiapuzi low-to-moderate hydrothermal Ag deposits, that are all located in the Qingchengzi orefield (Table 2). The mineralization ages (221–240 Ma) are consistent with the magmatic ages (210–230 Ma), suggestive of a magmatic-hydrothermal genesis for these deposits [8]. The Sr and Pb isotope characteristics of the deposits in the Qingchengzi orefield show that the ore-forming materials were derived from the magma and metamorphosed sequences [8,64]. The deposits of the Qingchengzi orefield are clustered in regions with high- ϵ_{Hf} (Figures 6, 8 and 9). This infers that the deposits are correlated to the magma, and that the magma is derived from the juvenile lower crust and the ancient lower crust (Figure 10a).

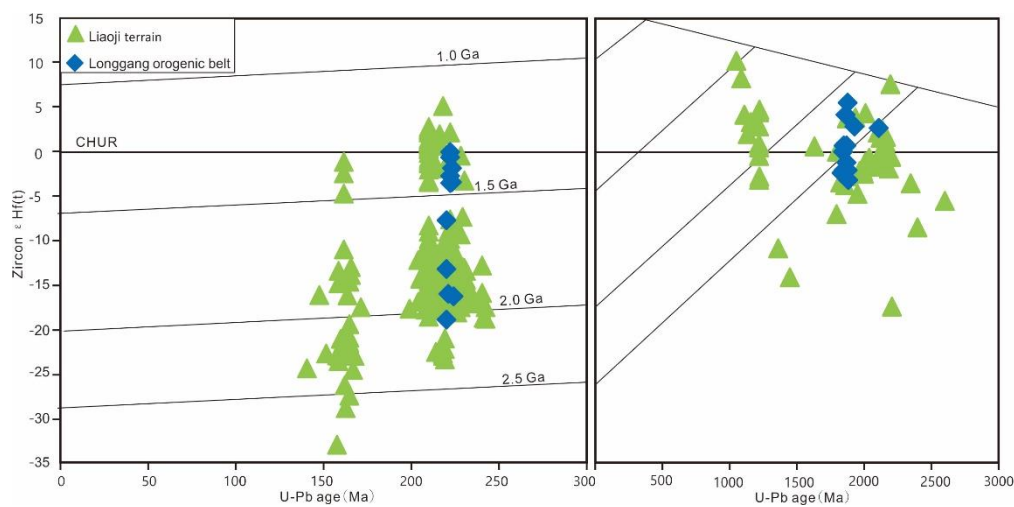


Figure 8. Plot of zircon U-Pb age versus $\epsilon_{\text{Hf}}(t)$ values for the magmatic rocks from the Liaodong Peninsula. Data are from Supplementary Material Table S2.

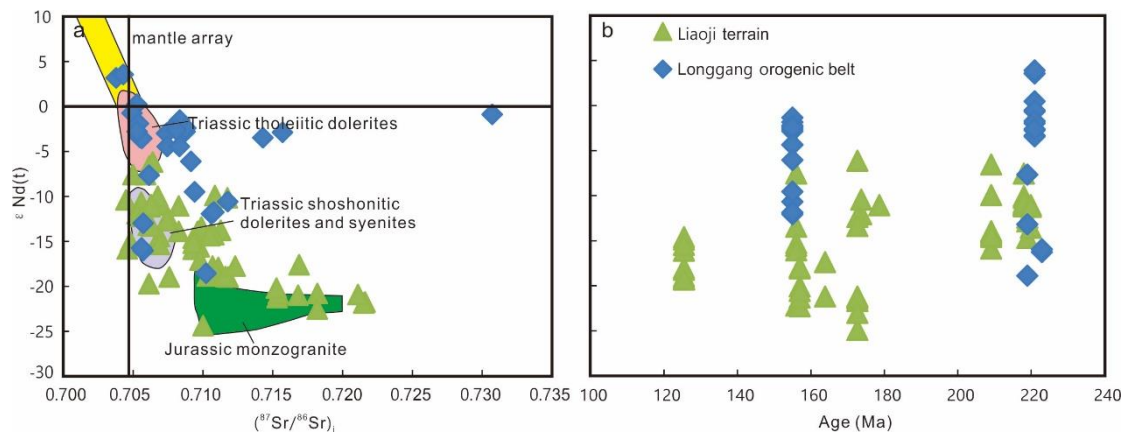


Figure 9. (a) Plot of whole-rock $(^{87}\text{Sr}/^{86}\text{Sr})_i$ versus $\epsilon_{\text{Nd}}(t)$ values for the magmatic rocks from the Liaodong Peninsula. (b) Plot of age versus whole-rock $\epsilon_{\text{Nd}}(t)$ values for the magmatic rocks from the Liaodong Peninsula. Data are from Supplementary Material Table S3.

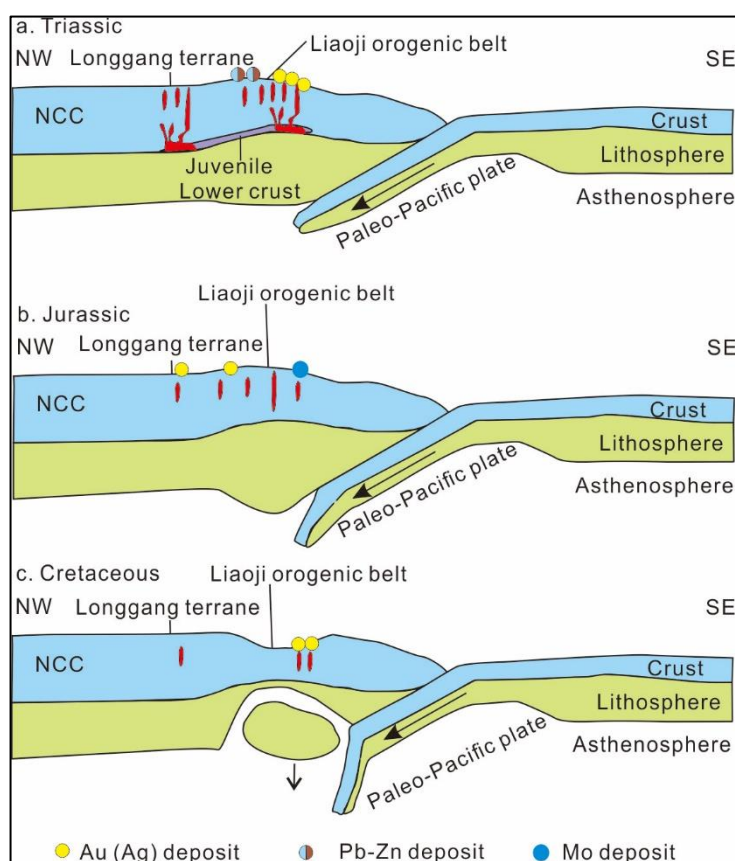


Figure 10. (a) Lithospheric architecture of the Liaodong Peninsula in the Triassic. (b) Lithospheric architecture of the Liaodong Peninsula in the Jurassic. (c) Lithospheric architecture of the Liaodong Peninsula in the Cretaceous.

In the Jurassic, the Maoling and Fenshui low-to-moderate hydrothermal Au deposits were formed in the Maoling orefield, and the Yaojiagou porphyry Mo deposit was formed in the Qingchengzi orefield (Table 2). Sulfur isotopes from the Miaoling deposit show typical magmatic sulfur characteristics [90]. The Pb isotope characteristics of the deposit show that the ore-forming materials came from the magma and the metamorphic sequences [90]. The deposits are clustered in regions with low ϵ_{Hf} and ϵ_{Nd} values (Figures 6–9). This infers that the deposits are correlated to the magma, which is derived from the ancient lower crust (Figure 10b).

The Cretaceous is another important metallogenic epoch. The Wulong orefield contains Wulong and Sidaogou low-to-moderate hydrothermal Au deposits. The characteristics of Sr and Pb isotopes suggest that the rock- and ore-forming and diagenetic materials of the Sanguliu granite near the Wulong orefield were derived from the magmatic rocks [62]. The H-O isotopes characteristics demonstrate that the ore-forming fluid came from magmatic fluid [62]. The deposits are clustered in regions with low ϵ_{Hf} and ϵ_{Nd} values (Figures 6–9). This infers that the deposits are correlated to the magma, which is derived from the ancient lower crust (Figure 10c).

6. Conclusions

In the Triassic, the Paleo-Pacific plate subducted beneath the NCC and caused the lithospheric thickening. The Triassic ore deposits are characterized by high $\epsilon_{\text{Hf}}(t)$ values, and are correlated to the magma, which is derived from the juvenile lower crust and the ancient lower crust. In the Jurassic, the lithospheric thickening continued. The Jurassic ore deposits are characterized by low $\epsilon_{\text{Hf}}(t)$ and ϵ_{Nd} values and are correlated to the magma derived from the ancient lower crust. In the Cretaceous, large-scale delamination may have taken place in this period. The Cretaceous ore deposits

are characterized by low $\epsilon\text{Hf}(t)$ and ϵNd values, and are correlated to the magma, which is derived from the ancient lower crust.

Supplementary Materials: The following are available online at <http://www.mdpi.com/2075-163X/9/3/179/s1>, Table S1: Major elements datas, Table S2: Hf isotope, Table S3: Sr-Nd isotope.

Author Contributions: Z.Z. and Y.W. conceived and designed the ideas; Z.Z. and D.L. collected and analyzed the data; Z.Z. wrote the manuscript; Y.W., D.L. and C.L. revised and edited the manuscript.

Funding: This study was financially supported by the National Key R&D Program of China (Grant No. 2018YFC0603804).

Acknowledgments: We thank the geologists from Team 103 of the Bureau of Non-ferrous Metal Geology (Dandong, Liaoning Province) for their field assistance.

Conflicts of Interest: The authors declare no conflict of interest.

References

1. Deng, J.; Wang, Q.F. Gold mineralization in China: Metallogenic provinces, deposit types and tectonic framework. *Gondwana Res.* **2016**, *36*, 219–274. [[CrossRef](#)]
2. Deng, J.; Liu, X.F.; Wang, Q.F.; Dilek, K.; Yang, L.Q. Isotopic characterization and petrogenetic modeling of early cretaceous mafic dike-lithospheric extension in the North China Craton, Eastern Asia. *GSA Bull.* **2017**, *129*, 1379–1407. [[CrossRef](#)]
3. Yang, L.Q.; Deng, J.; Guo, L.N.; Wang, Z.L.; Li, X.Z.; Li, J.L. Origin and evolution of ore fluid, and gold deposition processes at the giant Taishang gold deposit, Jiaodong Peninsula, Eastern China. *Ore Geol. Rev.* **2016**, *72*, 585–602. [[CrossRef](#)]
4. Yang, L.Q.; Deng, J.; Wang, Z.L.; Zhang, L.; Aufarb, R.J.; Yuan, W.M.; Weinberg, R.F.; Zhang, R.Z. Thermochronologic constraints on evolution of the Linglong Metamorphic Core Complex and implications for Au mineralization: A case study from the Xiadian Au deposit, Jiaodong Peninsula, eastern China. *Ore Geol. Rev.* **2016**, *72*, 165–178. [[CrossRef](#)]
5. Yang, L.Q.; Deng, J.; Wang, Z.L.; Guo, L.N.; Li, R.H.; Groves, D.I.; Danyushevsky, L.; Zhang, C.; Zheng, X.L.; Zhao, H. Relationships between gold and pyrite at the Xincheng gold deposit, Jiaodong Peninsula, China: Implications for gold source and deposition in a brittle epizonal environment. *Econ. Geol.* **2016**, *111*, 105–126. [[CrossRef](#)]
6. Yang, L.Q.; He, W.Y.; Gao, X.; Xie, S.X.; Yang, Z. Mesozoic multiple magmatism and porphyry-skarn Cu-polymetallic systems of the Yidun Terrane, Eastern Tethys: Implications for subduction- and transtension-related metallogeny. *Gondwana Res.* **2018**, *62*, 144–162. [[CrossRef](#)]
7. Wu, F.Y.; Yang, J.H.; Wilde, S.A.; Zhang, X.O. Geochronology, petrogenesis and tectonic implications of Jurassic granites in the Liaodong Peninsula, NE China. *Chem. Geol.* **2005**, *221*, 127–156. [[CrossRef](#)]
8. Yu, G.; Chen, J.F.; Xue, C.J.; Chen, Y.C.; Chen, F.K.; Du, X.Y. Geochronological framework and Pb, Sr isotope geochemistry of the Qingchengzi Pb-Zn-Ag-Au orefield, Northeastern China. *Ore Geol. Rev.* **2009**, *35*, 367–382. [[CrossRef](#)]
9. Duan, X.; Zeng, Q.; Yang, J.; Liu, J.; Wang, Y.; Zhou, L. Geochronology, geochemistry and Hf isotope of Late Triassic magmatic rocks of Qingchengzi district in Liaodong Peninsula, Northeast China. *J. Asian Earth Sci.* **2014**, *91*, 107–124. [[CrossRef](#)]
10. Zhang, P.; Li, B.; Li, J.; Chai, P.; Wang, X.; Sha, D.; Shi, J.M. Re-Os isotopic dating and its geological implication of gold bearing pyrite from the Baiyun gold deposit in Liaodong rift. *Geotecton. Metallog.* **2016**, *40*, 731–738. (In Chinese with English Abstract)
11. Wang, Y.W.; Xie, H.J.; Li, D.D.; Shi, Y.; Liu, F.X.; Sun, G.Q.; Sun, Q.M.; Zhou, G.C. Prospecting prediction of ore concentration area exemplified by Qingchengzi Pb-Zn-Au-Ag ore concentration area, Eastern Liaoning Province. *Miner. Depos.* **2017**, *36*, 1–24. (In Chinese with English Abstract)
12. Yang, J.H.; Sun, J.F.; Zhang, J.H.; Wilde, S.A. Petrogenesis of Late Triassic intrusive rocks in the Northern Liaodong Peninsula related to decratonization of the North China Craton: Zircon U-Pb age and Hf-O isotope evidence. *Lithos* **2012**, *153*, 108–128. [[CrossRef](#)]

13. Xiao, S.Y.; Zhu, G.; Zhang, S.; Liu, C.; Su, N.; Yi, H.; Wu, X.D.; Li, Y.J. Structural processes and dike emplacement mechanism in the Wulong gold field, eastern Liaoning. *Chin. Sci. Bull.* **2018**, *63*, 3022–3036. (In Chinese with English Abstract) [[CrossRef](#)]
14. Li, S.Z.; Liu, J.Z.; Zhao, G.C.; Wu, F.Y.; Han, Z.Z.; Yang, Z.Z. Key geochronology of Mesozoic deformation in the eastern block of the North China Craton and its constraints on regional tectonics: A case of Jiaodong and Liaodong Peninsula. *Acta Petrol. Sin.* **2004**, *20*, 633–646. (In Chinese with English Abstract)
15. Deng, J.; Wang, Q.F.; Li, G.J. Tectonic evolution, superimposed orogeny, and composite metallogenic system in China. *Gondwana Res.* **2017**, *50*, 216–266. [[CrossRef](#)]
16. Deng, J.; Yang, L.Q.; Li, R.H.; Groves, D.I.; Santosh, M.; Wang, Z.L.; Sai, S.X.; Wang, S.R. Regional structural control on the distribution of world-class gold deposits: An overview from the giant Jiaodong Gold Province. *China Geol. J.* **2017**. [[CrossRef](#)]
17. Yang, L.Q.; Deng, J.; Qiu, K.F.; Ji, X.Z.; Santosh, M.; Song, K.R.; Song, Y.H.; Geng, J.Z.; Zhang, C.; Hua, B. Magma mixing and crust-mantle interaction in the Triassic monzogranites of Bikou Terrane, central China: Constraints from petrology, geochemistry, and zircon U-Pb-Hf isotopic systematics. *J. Asian Earth Sci.* **2015**, *98*, 320–341. [[CrossRef](#)]
18. Yang, L.Q.; Guo, L.N.; Wang, Z.L.; Zhao, R.X.; Song, M.C.; Zheng, X.L. Timing and mechanism of gold mineralization at the Wang’ershan gold deposit, Jiaodong Peninsula, Eastern China. *Ore Geol. Rev.* **2017**, *88*, 491–510. [[CrossRef](#)]
19. Griffin, W.L.; Wang, X.; Jackson, S.E.; Pearson, N.J.; O’Reilly, S.Y.; Xu, X.S.; Zhou, X.M. Zircon chemistry and magma mixing, SE China: In-situ analysis of Hf isotopes, Tonglu and Pingtan igneous complexes. *Lithos* **2002**, *61*, 237–269. [[CrossRef](#)]
20. Griffin, W.L.; Belousova, E.A.; Shee, S.R.; Pearson, N.J.; O’Reilly, S.Y. Archean crustal evolution in the northern Yilgarn Craton: U-Pb and Hf-isotope evidence from detrital zircons. *Precambrian Res.* **2004**, *131*, 231–282. [[CrossRef](#)]
21. Kemp, A.I.S.; Hawkesworth, C.J.; Paterson, B.A.; Kinny, P.D. Episodic growth of the Gondwana supercontinent from hafnium and oxygen isotopes in zircon. *Nature* **2006**, *439*, 580–583. [[CrossRef](#)] [[PubMed](#)]
22. McCuaig, T.C.; Beresford, S.; Hronsky, J. Translating the mineral systems approach into an effective exploration targeting system. *Ore Geol. Rev.* **2010**, *38*, 128–138. [[CrossRef](#)]
23. Mole, D.R.; Fiorentini, M.L.; Thebaud, N.; McCuaig, T.C.; Cassidy, K.F.; Kirkland, C.L.; Wingate, M.T.D.; Romano, S.S.; Doublier, M.P.; Belousova, E.A. Spatiotemporal constraints on lithospheric development in the Southwest-Central Yilgarn Craton, Western Australia. *Australian. J. Earth Sci.* **2012**, *59*, 625–656.
24. Mole, D.R.; Fiorentini, M.L.; Thebaud, N.; Cassidy, K.F.; McCuaig, T.C.; Kirkland, C.L.; Romano, S.S.; Doublier, M.P.; Belousova, E.A.; Barnes, S.J.; et al. Archean komatiite volcanism controlled by the evolution of early continents. *Proc. Natl. Acad. Sci. USA* **2014**, *111*, 10083–10088. [[CrossRef](#)] [[PubMed](#)]
25. Mole, D.R.; Fiorentini, M.L.; Cassidy, K.F.; Kirkland, C.L.; Romano, N.; Maas, R.; Belousova, E.A.; Barnes, S.J.; Mill, J. Crustal Evolution, Intra-cratonic Architecture and the Metallogeny of an Archaean Craton. *Geol. Soc. Lond. Spec. Pub.* **2015**, *393*, 23–80. [[CrossRef](#)]
26. Belousova, E.A.; Kostitsyn, Y.A.; Griffin, W.L.; Begg, G.C.; O’Reilly, S.Y.; Pearson, N.J. The growth of the continental crust: Constraints from zircon Hf-isotope data. *Lithos* **2010**, *119*, 457–466. [[CrossRef](#)]
27. Hou, Z.Q.; Duan, L.F.; Lu, Y.J.; Zheng, Y.C.; Zhu, D.C.; Yang, Z.M.; Yang, Z.S.; Wang, B.D.; Pei, Y.R.; Zhao, Z.D.; et al. Lithospheric architecture of the Lhasa Terrane and its control on ore deposits in the Himalayan-Tibetan Orogen. *Econ. Geol.* **2015**, *110*, 1541–1575. [[CrossRef](#)]
28. Wang, C.M.; Bagas, L.; Lu, Y.J.; Santosh, M.; Du, B.; McCuaig, T.C. Terrane boundary and spatio-temporal distribution of ore deposits in the Sanjiang Tethyan Orogen: Insights from zircon Hf-isotopic mapping. *Earth-Sci. Rev.* **2016**, *156*, 39–65. [[CrossRef](#)]
29. Wang, C.M.; Deng, J.; Bagas, L.; Wang, Q.F. Zircon Hf-isotopic mapping for understanding crustal architecture and metallogenesis in the Eastern Qinling Orogen. *Gondwana Res.* **2017**, *50*, 293–310. [[CrossRef](#)]
30. Yang, J.H.; Wu, F.Y.; Wilde, S.A.; Liu, X.M. Petrogenesis of Late Triassic granitoids and their enclaves with implications for post-collisional lithospheric thinning of the Liaodong Peninsula, North China Craton. *Chem. Geol.* **2007**, *242*, 155–175. [[CrossRef](#)]
31. Suo, A.; Zhao, D.Z.; Zhang, F.S.; Wang, H.R.; Liu, F.Q. Driving forces and management strategies for estuaries in Northern China. *Front. Earth Sci. China* **2010**, *4*, 51–58. [[CrossRef](#)]

32. Yang, J.H.; Wu, F.Y.; Chung, S.L.; Wilde, S.A.; Chu, M.F. A hybrid origin for the Qianshan A-type granite, Northeast China: Geochemical and Sr-Nd-Hf isotopic evidence. *Lithos* **2006**, *89*, 89–106. [[CrossRef](#)]
33. Li, S.Z.; Zhao, G.C.; Santosh, M.; Liu, X.; Dai, L.M. Palaeoproterozoic tectonothermal evolution and deep crustal processes in the Jiao-Liao-Ji belt, North China Craton: A review. *Geol. J.* **2011**, *46*, 525–543. [[CrossRef](#)]
34. Wang, Y.; Wang, F.; Wu, L.; Shi, W.; Yang, L. (U-Th)/He thermochronology of metallic ore deposits in the Liaodong Peninsula: Implications for orefield evolution in Northeast China. *Ore Geol. Rev.* **2018**, *92*, 348–365. [[CrossRef](#)]
35. Jiang, Y.H.; Jiang, S.Y.; Ling, H.F.; Ni, P. Petrogenesis and tectonic implications of Late Jurassic shoshonitic lamprophyre dikes from the Liaodong Peninsula, NE China. *Miner. Petrol.* **2010**, *100*, 127–151. [[CrossRef](#)]
36. Yang, F.C.; Song, Y.H.; Hao, L.B.; Chai, P. Late Jurassic shrimp U-Pb age and Hf isotopic characteristics of granite from the Sanjiazi area in Liaodong and their geological significance. *Acta Geol. Sin.* **2015**, *89*, 1773–1782. (In Chinese with English Abstract)
37. Pei, F.P. Zircon U-Pb Chronology and Geochemistry of Mesozoic Intrusive Rocks in Southern Liaoning and Jilin Provinces: Constraints on the Spatial-Temporal Extent of the North China Craton Destruction. Ph.D. Thesis, Jilin University, Changchun, China, 2008. (In Chinese with English Abstract).
38. Li, C.; Chen, B.; Li, Z.; Yang, C. Petrologic and geochemical characteristics of Paleoproterozoic monzogranitic gneisses from Xiuyan-Kuandian area in Liaodong Peninsula and their tectonic implications. *Acta Petrol. Sin.* **2017**, *33*, 963–977. (In Chinese with English Abstract)
39. Song, Y.; Yang, F.; Yan, G.; Wei, M.; Shi, S. Shrimp U-Pb ages and Hf isotopic compositions of Paleoproterozoic granites from the Eastern part of Liaoning Province and their tectonic significance. *Acta Geol. Sin.* **2016**, *90*, 2620–2636. (In Chinese with English Abstract)
40. Luo, Y.; Sun, M.; Zhao, G.C.; Li, S.Z.; Xu, P.; Ye, K.; Xia, X.P. LAICP-MS U-Pb zircon ages of the Liaohe Group in the Eastern Block of the North China Craton, constraints on the evolution of the Jiao-Liao-Ji Belt. *Precambrian Res.* **2004**, *134*, 349–371. [[CrossRef](#)]
41. Liu, J.L.; Ji, M.; Shen, L.; Guan, H.M.; Davis, G.A. Early Cretaceous extensional structures in the Liaodong peninsula: Structural associations, geochronological constraints and regional tectonic implications. *Sci. China* **2011**, *54*, 823–842. [[CrossRef](#)]
42. Wu, F.Y.; Lin, J.Q.; Wilde, S.A.; Zhang, X.O.; Yang, J.H. Nature and significance of the Early Cretaceous giant igneous event in Eastern China. *Earth Planet. Sci. Lett.* **2005**, *233*, 103–119. [[CrossRef](#)]
43. Yang, J.H.; Wu, F.Y.; Wilde, S.A. A review of the geodynamic setting of large-scale late mesozoic gold mineralization in the North China Craton: An association with lithospheric thinning. *Ore Geol. Rev.* **2003**, *23*, 125–152. [[CrossRef](#)]
44. Yu, G.; Yang, G.; Chen, J.; Qu, W.; Du, A.; He, W. Re-Os dating of gold-bearing arsenopyrite of the Maoling gold deposit, Liaoning province, Northeast China and its geological significance. *Chin. Sci. Bull.* **2005**, *50*, 1509–1514. [[CrossRef](#)]
45. Dai, J.Z. Characteristics of ore-forming fluids and discussion on the genesis of Au, Ag deposits in Qingchengzi region, Liaoning province. Master Dissertation, Jilin University, Changchun, China, 2005. (In Chinese with English abstract).
46. Li, D.D.; Wang, Y.W.; Zhou, G.C.; Shi, Y.; Xie, H.J. Preliminary analysis of the relationship between dikes and gold mineralization in Baiyun gold deposit, Liaoning. *Miner. Explor.* **2016**, *7*, 113–119, (In Chinese with English abstract).
47. Jing, Y.; Jiang, S.; Zhao, K.; Ni, P.; Ling, H.; Liu, D. Shrimp U-Pb zircon dating for lamprophyre from Liaodong Peninsula: Constraints on the initial time of Mesozoic lithosphere thinning beneath Eastern China. *Sci. Bull.* **2005**, *50*, 2612–2620. [[CrossRef](#)]
48. Liu, J.L.; Sun, F.Y.; Zhang, Y.J.; Ma, F.; Liu, F.X.; Zeng, L. Zircon U-Pb Geochronology, Geochemistry and Hf Isotopes of Nankouqian Granitic Intrusion in Qingyuan Region, Liaoning Province. *Earth Sci.* **2016**, *41*, 55–66. (In Chinese with English Abstract)
49. Song, J.Q. Geochemistry and Chronology of Alkaline Rocks in Fengcheng, Liaodong and Their Geological Implications. Master's Thesis, China University of Geosciences, Beijing, China, 2017. (In Chinese with English Abstract).
50. Li, S.Z.; Zhao, G.C. SHRIMP U-Pb zircon geochronology of the Liaoji granitoids: Constraints on the evolution of the Paleoproterozoic Jiao-Liao-Ji belt in the Eastern Block of the North China Craton. *Precambrian Res.* **2007**, *158*, 1–16. [[CrossRef](#)]

51. Ma, Y.B.; Bagas, L.; Xing, S.W.; Zhang, S.T.; Wang, R.J.; Li, N.; Zhang, Z.J.; Zou, Y.F.; Yang, X.Q.; Wang, Y.; et al. Genesis of the stratiform Zhenzigou Pb Zn deposit in the North China Craton: Rb Sr and C O S Pb isotope constraints. *Ore Geol. Rev.* **2016**, *79*, 88–104. [[CrossRef](#)]
52. Liu, G.P.; Ai, Y.F. Metamorphic rock-hosted disseminated gold deposits—A case study of the xiaotongjiapuzi gold deposit of eastern liaoning. *Acta Geol. Sin.-Engl.* **1999**, *73*, 429–437.
53. Xu, S.; Wang, M.; Liu, C.C.; Li, S.Y. Evaluation of gold geochemical anomalies in the liaodong paleorift. *Appl. Mech. Mater.* **2014**, *484–485*, 620–627. [[CrossRef](#)]
54. Chen, J.F.; Yu, G.; Xue, C.J.; Qian, H.; He, J.F.; Xing, Z.; Zhang, X. Pb isotope geochemistry of lead, zinc, gold and silver deposit clustered region, Liaodong rift zone, Northeastern China. *Sci. China* **2005**, *48*, 467–476. [[CrossRef](#)]
55. Zhang, W.Q.; Zheng, T.; Zhang, X.; Xu, D.N. Geological characteristics and metallogenic mechanism of Yangshu large-scale Au-Ag deposits in Qingchengzi orefield primary study. *Non-Ferr. Min. Metall.* **2007**, *23*, 4–6. (In Chinese with English Abstract)
56. Sun, G.Q.; Sun, Q.M.; Zheng, T. Geological characteristics and metallogenic mechanism of the Taoyuan gold deposit in Qingchengzi ore field, Liaoning. *Gansu Metall.* **2008**, *30*, 49–51. (In Chinese with English Abstract)
57. Fang, J.Q.; Nie, F.J.; Zhang, K.; Liu, Y.; Xu, B. Re-Os isotopic dating on molybdenite separates and its geological significance from the Yaojiagou molybdenum deposit, Liaoning Province. *Acta Petrol. Sin.* **2012**, *28*, 372–378. (In Chinese with English Abstract)
58. He, C.Z. The Characteristics of Metallogenic Fluid and Depths of Yaojiagou Porphyry-Mo Deposit in Qingchengzi Town, Liaoning Province. Master's Thesis, China University of Geosciences, Beijing, China, 2015. (In Chinese with English Abstract).
59. Yu, B.; Zeng, Q.D.; Frimmel, H.E.; Wang, Y.B.; Guo, W.K.; Sun, G.T.; Zhou, T.C.; Li, J.P. Genesis of the Wulong gold deposit, northeastern North China Craton: Constraints from fluid inclusions, H-O-S-Pb isotopes, and pyrite trace element concentrations. *Ore Geol. Rev.* **2018**, *102*, 313–337. [[CrossRef](#)]
60. Hao, R.X.; Peng, S.L. Geochemical study of Wangjiawaizi gold deposit in Liaoning. *Gold Geol.* **1999**, *5*, 47–51. (In Chinese with English Abstract)
61. Qu, F.F. Geology and genesis of Fenshui gold deposit. *J. Precious Met. Geol.* **2003**, *12*, 85–91. (In Chinese with English Abstract)
62. Wei, J.H.; Liu, C.Q.; Tang, H.F. Rb-Sr and U-Pb isotopic systematics of pyrite and granite in Liaodong gold province, North, China: Implication for the age and genesis of a gold deposit. *Geochem. J.* **2003**, *37*, 567–577. [[CrossRef](#)]
63. Zhou, G.C. Study on the Genesis of the Baiyun Gold Deposit in Liaodong, Liaoning Province. Master's Thesis, Kunming University of Science and Technology, Kunming, China, 2017. (In Chinese with English Abstract).
64. Liu, J.; Liu, F.X.; Li, S.H.; Lai, C.K. Formation of the Baiyun gold deposit, Liaodong gold province, NE China: Constraints from zircon U-Pb age, fluid inclusion, and C-H-O-Pb-He isotopes. *Ore Geol. Rev.* **2019**, *104*, 628–655. [[CrossRef](#)]
65. Qiu, K.F.; Taylor, R.D.; Song, Y.H.; Yu, H.C.; Song, K.R.; Li, N. Geologic and geochemical insights into the formation of the taiyangshan porphyry copper-molybdenum deposit, western qinling orogenic belt, China. *Gondwana Res.* **2016**, *35*, 40–58. [[CrossRef](#)]
66. Geng, J.Z.; Qiu, K.F.; Gou, Z.Y.; Yu, H.C. Tectonic regime switchover of Triassic Western Qinling orogen: Constraints from LA-ICP-MS zircon U-Pb geochronology and Lu-Hf isotope of Dangchuan intrusive complex in Gansu, China. *Chem. Erde Geochem.* **2017**, *77*, 637–651. [[CrossRef](#)]
67. Qiu, K.F.; Yu, H.C.; Gou, Z.Y.; Liang, Z.L.; Zhang, J.L.; Zhu, R. Nature and origin of triassic igneous activity in the western qinling orogen: The wenquan composite pluton example. *Int. Geol. Rev.* **2018**, *60*, 242–266. [[CrossRef](#)]
68. Scherer, E.; Münker, C.; Mezger, K. Calibration of the lutetium-hafnium clock. *Science* **2001**, *293*, 683–687. [[CrossRef](#)] [[PubMed](#)]
69. Blichert-Toft, J.; Albarède, F. The Lu-Hf isotope geochemistry of chondrites and the evolution of themantle-crust system. *Earth Planet. Sci. Lett.* **1997**, *148*, 243–258. [[CrossRef](#)]
70. Bouvier, A.; Vervoort, J.D.; Patchett, P.J. The Lu-Hf and Sm-Nd isotopic composition of CHUR: Constraints from unequilibrated chondrites and implications for the bulk composition of terrestrial planets. *Earth Planet. Sci. Lett.* **2008**, *273*, 48–57. [[CrossRef](#)]

71. Qiu, K.F.; Deng, J.; Taylor, R.D.; Song, K.R.; Song, Y.H.; Li, Q.Z.; Goldfarb, R.J. Paleozoic magmatism and porphyry Cu-mineralization in an evolving tectonic setting in the north qilian orogenic belt, nw china. *J. Asian Earth Sci.* **2016**, *122*, 20–40. [[CrossRef](#)]
72. Qiu, K.F.; Deng, J. Petrogenesis of granitoids in the dewulu skarn copper deposit: Implications for the evolution of the paleotethys ocean and mineralization in western qinling, china. *Ore Geol. Rev.* **2017**, *99*, 1078–1098. [[CrossRef](#)]
73. Erdogan, S. A comparison of interpolation methods for producing digital elevation models at the field scale. *Earth Surf. Proc. Land.* **2010**, *34*, 366–376. [[CrossRef](#)]
74. Deng, J.; Wang, C.M.; Bagas, L.; Santosh, M.; Yao, E. Crustal architecture and metallogenesis in the south-eastern North China Craton. *Earth-Sci. Rev.* **2018**, *182*, 251–272. [[CrossRef](#)]
75. Gao, X.; Yang, L.Q.; Orovan, E.A. The lithospheric architecture of two subterrane in the eastern Yidun Terrane, East Tethys: Insights from Hf-Nd isotopic mapping. *Gondwana Res.* **2018**. [[CrossRef](#)]
76. Wang, C.M.; Bagas, L.; Deng, J.; Dong, M. Crustal architecture and its controls on mineralization in the North China Craton. *Ore Geol. Rev.* **2018**. [[CrossRef](#)]
77. Li, H.Y.; Xu, Y.G.; Liu, Y.M.; Huang, X.L.; He, B. Detrital zircons reveal no Jurassic plateau in the Eastern North China Craton. *Gondwana Res.* **2013**, *24*, 622–634. [[CrossRef](#)]
78. Hall, H.C.; Fahrig, W.F. Mafic dyke swarms. *Geol. Assoc. Can. Spec.* **1987**, *34*, 1–503.
79. Zhao, J.X.; McCulloch, M.T. Melting of a subduction-modified continental lithospheric mantle, evidence from late Proterozoic mafic dike swarms in central Australia. *Geology* **1993**, *21*, 463–466. [[CrossRef](#)]
80. Rowley, D.B.; Xue, F.; Tucker, R.D.; Peng, Z.X.; Baker, J.; Davis, A. Ages of ultrahigh pressure metamorphism and protolith orthogneisses from the Eastern Dabie Shan: U/Pb zircon geochronology. *Earth Planet. Sci. Lett.* **1997**, *151*, 191–203. [[CrossRef](#)]
81. Li, S.G.; Jagoutz, E.; Chen, Y. Sm-Nd and Rb-Sr isotopic chronology and cooling history of ultrahigh pressure metamorphic rocks and their country rocks at Shuanghe in the Dabie Mountains, central China. *Geochim. Cosmochim. Acta* **2000**, *64*, 1077–1093. [[CrossRef](#)]
82. Wan, Y.S.; Li, R.W.; Wilde, S.A.; Liu, D.Y.; Chen, Z.Y.; Yan, L.; Song, T.R.; Yin, X.Y. UHP metamorphism and exhumation of the Dabie Orogen, China, evidence from SHRIMP dating of zircon and monazite from UHP granitic gneiss cobble from the Hefei Basin. *Geochim. Cosmochim. Acta* **2005**, *69*, 4333–4348. [[CrossRef](#)]
83. Yang, J.H.; O'reilly, S.; Walker, R.J.; Griffin, W.; Wu, F.Y.; Zhang, M.; Pearson, N. Diachronous decratonization of the Sino-Korean Craton, geochemistry of mantle xenoliths from North Korea. *Geology* **2010**, *38*, 799–802. [[CrossRef](#)]
84. Gilder, S.A.; Gill, J.; Coe, R.S.; Zhao, X.X.; Liu, Z.; Wang, G. Isotopic and paleomagnetic constraints on the Mesozoic tectonic evolution of south China. *Geophys. Res.* **1996**, *101*, 16137–16154. [[CrossRef](#)]
85. Zhou, X.M.; Li, W.X. Origin of Late Mesozoic igneous rocks in Southeastern China: Implications for lithosphere subduction and underplating of mafic magmas. *Tectonophysics* **2000**, *326*, 269–287. [[CrossRef](#)]
86. Wang, R.; Tafti, R.; Hou, Z.Q.; Shen, Z.C.; Guo, N.; Evans, N.J.; Jeon, H.; Li, Q.Y.; Li, W.K. Across-arc geochemical variation in the Jurassic magmatic zone, Southern Tibet: Implication for continental arc-related porphyry Cu-Au mineralization. *Chem. Geol.* **2017**, *451*, 116–134. [[CrossRef](#)]
87. Li, X.H.; Chen, Z.G.; Liu, D.Y.; Li, W.X. Jurassic gabbro-granite-syenite suites from southern Jiangxi Province, SE China: Age, origin, and tectonic significance. *Int. Geol. Rev.* **2003**, *45*, 898–921. [[CrossRef](#)]
88. Zhuang, L.; Pei, F.P.; Meng, E. Zircon U-Pb age, geochemical and Nd isotopic data of Middle Jurassic high-mg dioritic dike in Liaodong peninsula, NE China. *Glob. Geol.* **2014**, *17*, 143–154.
89. Wilde, S.A.; Zhou, X.H.; Nemchin, A.A.; Sun, M. Mesozoic crust-mantle interaction beneath the North China craton: A consequence of the dispersal of Gondwanaland and accretion of Asia. *Geology* **2003**, *31*, 817–820. [[CrossRef](#)]
90. Zhang, P.; Zhao, Y.; Kou, L.L.; Bi, Z.W.; Yang, H.Z. Sulfur-lead Isotopic Composition of the Maoling Gold Deposit in Liaodong, and its Geological Implications. *Geol. Rev.* **2017**, *63*, 175–176. (In Chinese with English Abstract)

